# Passive submillimeter-wave imaging demonstrated by a two-element interferometer Postprint

**Authors:** Han, Dong-Hao, Liu, Hao, Zhang, De-Hai, Jin Meng, Zhao, Xin, Zhang, Ying, Wu, Ji

**Date:** 2017-03-10T00:00:00+00:00

## Abstract

In this paper, an SMMW interferometric radiometer concept is demonstrated by a two-element interferometer with dedicated high accuracy SMMW devices. Point-source calibration method is introduced in order to reduce instrument errors. Interference fringes and point target images are presented by this SMMW interferometer. The linear phase error of the interference fringes is less than 2° and the angular resolution is better than 0.57°. The measured performance characteristics of the two-element interferometer are consistent with the theoretical analysis. This interferometer demonstrates a new method for passive SMMW remote sensing. 

## Full Text

### Passive Submillimeter-Wave Imaging Demonstrated by Two-Element Interferometer

**Donghao Han[1,2], Hao Liu[1], Dehai Zhang[1], Jin Meng[1], Xin Zhao[1], Ying Zhang[1,2], Ji Wu[1]**

[1] National Space Science Center, Chinese Academy of Sciences, Beijing 100190, China
[2] University of Chinese Academy of Sciences, Beijing 100049, China

E-mail: liuhao@mirslab.cn

#### Abstract

Interferometric radiometer obtains passive brightness temperature images by correlation operation between different receivers, which would seriously increase hardware requirements and need high phase accuracy in submillimeter-wave (SMMW) spectral region. An interferometric radiometer based on two-element interferometer has been set up with specialized high accuracy SMMW devices in this paper. Point-source target calibration has been introduced to reduce instrumental error. Interference fringes and point target images are presented by this SMMW interferometer. The linear phase error of interference fringes is better than 2°. The angular resolution is 0.57°. System performance is in accord with theoretical analysis. This interferometer demonstrates a new way for passive SMMW remote sensing.

**PACS:** 07.57.Kp

**Key words:** submillimeter-wave (SMMW) imaging, point-source target calibration, SMMW interference fringes, interferometric radiometer

---

**Abstract (Chinese Translation)**

Interferometric radiometers obtain passive brightness temperature images through correlation operations between multiple channels. For the submillimeter-wave (SMMW) band, the correlation operation imposes stringent requirements on the precision and phase stability of the hardware system. In this paper, a set of interferometric radiometer system based on a two-element interferometer is implemented through specially designed high-precision SMMW devices. A point-source target response calibration method is proposed to reduce system errors according to the characteristics of this system. After the system was completed, interference fringe experiments and point-source target imaging experiments were carried out respectively. Tests show that the linear phase error of the system is less than 2°, and the angular resolution is better than 0.57°. The measured system performance is consistent with theoretical analysis results. The above research provides important reference value for the future design of high-resolution submillimeter-wave interferometric imaging radiometers.

**Key words:** Submillimeter-wave imaging, point-source target response calibration, submillimeter-wave interference fringes, interferometric

---

## Introduction

The submillimeter-wave (SMMW) spectral region, commonly spanning from 300 GHz to 3000 GHz, represents one of the most exciting yet frustrating sectors of the electromagnetic spectrum. It is exciting because of the wealth of knowledge that can be gained from research at these frequencies, yet frustrating because techniques have lagged behind those at lower and higher frequencies [1]. With recent technological advances [2], SMMW detectors are playing an increasingly important role in remote sensing applications [3], such as security detection [4] and meteorological observation [5].

In geoscience applications [6], many molecules have characteristic absorption lines in the SMMW spectral region; for example, 380 GHz corresponds to water vapor absorption spectra, and 425 GHz to oxygen absorption spectra. Numerous attempts have been made to exploit the SMMW electromagnetic spectrum, with several successful missions including Aura [7] and SMILES [8]. The Geostationary Interferometric Microwave Sounder (GIMS) [9] is a millimeter-wave imaging sounder concept proposed for China' s next-generation geostationary meteorological satellite (FY-4M). Some millimeter-wave (MMW) bands, such as 50–56 GHz and 183 GHz, have been developed for GIMS [10]. Due to its short wavelength, SMMW spectra are also fascinatingly helpful for GIMS to increase spatial resolution, which is crucial for geostationary remote sensing.

Most existing SMMW sensors are based on either spatial domain scanning imaging or focal plane array imaging. Spatial domain scanning imaging systems have simple hardware structures but require large antenna apertures and long imaging periods, as exemplified by the Microwave Limb Sounder (MLS) on Aura [7][11]. On the other hand, focal plane arrays can decrease imaging time but sharply increase hardware costs, as is the case with the Heterodyne Instrument for the Far-Infrared (HIFI) on Herschel [12]. Unlike these instruments, interferometric radiometers synthesize a large antenna aperture using multiple small antennas, and are thus also called synthetic aperture radiometers [13]. Spatial frequency domain sampling is accomplished by moving receivers, enabling a flexible tradeoff between system complexity and imaging period. Unlike traditional radiometers, correlation measurement in interferometric radiometers requires phase information between receivers [14][15]. This means high hardware stability and phase accuracy must be achieved in the SMMW spectral region because the short wavelength is extremely sensitive to delay error. To the best of our knowledge based on public reporting, the highest frequency of existing interferometric imaging radiometers is 183 GHz, realized by the GeoSTAR project [16].

In this paper, a passive SMMW interferometric radiometer is established using a two-element interferometer operating at 440 GHz. Due to its system similarities, this SMMW interferometric radiometer will be compatible with GIMS and other spectral instruments. Related SMMW services with high stability are developed for this interferometric radiometer to ensure hardware stability and phase accuracy in the SMMW spectral region [17][18]. Furthermore, a new calibration method—point-source target calibration—is introduced to eliminate instrumental errors. In Section 1, the observation is formulated for the interferometric radiometer. The two-element SMMW interferometer and the point-source target calibration are presented in Section 2. Section 3 demonstrates the interference fringes and point target images obtained with this SMMW interferometer, followed by conclusions and outlook in Section 4.

---

## 1 Formulation for Interferometric Imaging

An elementary interferometer of an interferometric radiometer [13] is shown in Figure 1

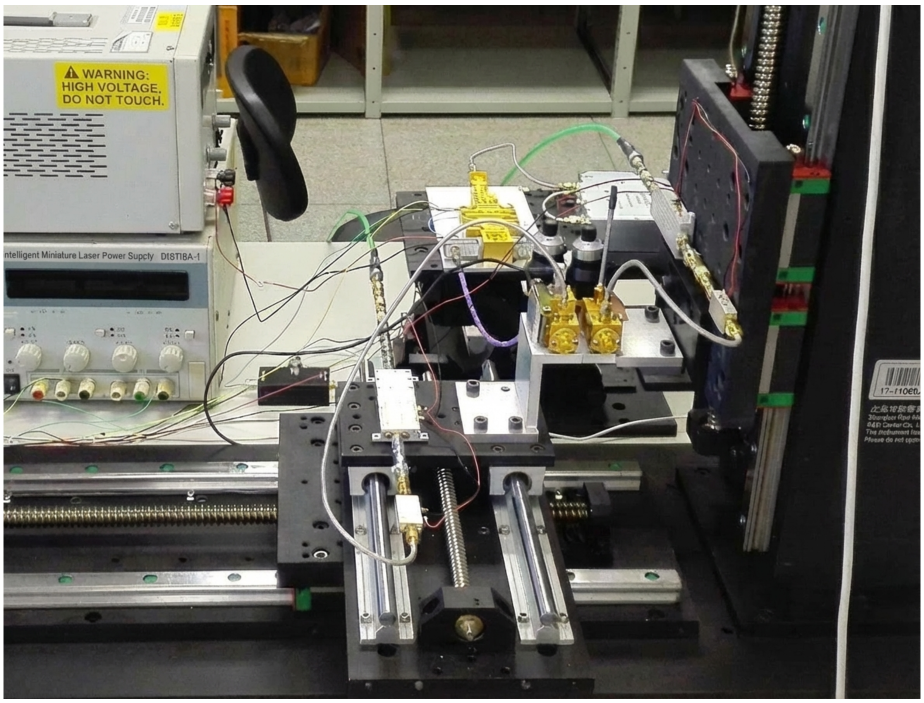


Figure 1: Figure 1

. The two antennas are separated by a distance $D$, defined as the baseline, and observe a point source located at direction $s$, which is in the far field of the interferometer. Thus, the incident wavefront can be considered planar over the distance $D$. To simplify the discussion, the receivers are assumed to have narrow bandpass filters that pass only signal components very close to frequency $f$ . The output in Figure 1 can be described as:

$$V_i \propto \langle A \sin(2\pi f t + \varphi) \cdot A \sin(2\pi f(t - \tau_g) + \varphi) \rangle = A^2 \cos(2\pi \sin\theta \cdot D/\lambda)$$

where $A$ is the signal strength of the point source,   is the wavelength corresponding to $f$ , and  _g is the time delay between the two receivers. The quadrature component  V_q can be obtained similarly. When the source becomes an area target expressed as  T( ,  ), and practical bandwidths are considered in the receivers, the output of the elementary interferometer can be described as [19]:

$$V(u,v) = \iint_{\xi^2+\eta^2\leq 1} T(\xi,\eta)\cdot F^*_{1,2}(\xi,\eta)\cdot r_{1,2}(\xi,\eta)\cdot \tilde{r}(u,v)e^{-j2\pi(u\xi+v\eta)}\,d\xi\,d\eta$$

Here, $u$ and $v$ are the projections of the baseline normalized to the wavelength over the X-Y axes. *T_r* is the instrument temperature. $F$ , *( , )* is the conjugate product of the receiver antenna patterns for receivers 1 and 2. $\tilde{r}$ , ( , ) is the fringe washing function related to the receiver frequency response [20]. *V_i* and *V_q* correspond to the real and imaginary parts of *V(u,v)*, respectively.

By changing baseline $D$, the synthetic aperture interferometric radiometer can sample the effective spatial frequency domain. Then *T( , )* can be inverted by appropriate inverse algorithms [21][22].

---

## 2 System Architecture

This SMMW interferometric radiometer is constructed using a two-element interferometer. Because short wavelengths are very sensitive to delay error, correlation for the interferometer requires not only high hardware stability but also high phase accuracy. Therefore, SMMW devices must be elaborately designed in the front end, and a high-speed digital correlator is employed in the back end. Moreover, a new calibration method—point-source target calibration—is proposed to eliminate instrumental errors.

### A. Modular Composition

This SMMW interferometer mainly consists of three parts: an antenna subsystem, an analog front-end subsystem, and a digital correlator. Additionally, a two-dimensional moving platform is employed to complete spatial frequency domain scanning. The integrated system is shown in Figure 2 [FIGURE:2]. In Figure 2(a), the dash line with arrows indicates flexible waveguide connections. Two receivers are fixed respectively on the two moving arms of the platform. One arm can move horizontally and the other vertically, so the trace of these arms is T-shaped—hence the term T-shaped scanning. The SMMW interferometer and moving platform are shown in Figure 2(b).

Horn antennas are employed in this system, which offer mature technology and high reliability. The antenna gain is 25.6 dB, the 3 dB beamwidth is 10°, the sidelobe level is lower than -30 dB, and the cross-polarization level is better than 30 dB.

The analog subsystem mainly includes three components: a local oscillator (LO), a tripler, and a mixer. Considering current processing technology levels, a circuit structure of anti-parallel diodes with self-bias is proposed for the tripler [17], as shown in Figure 3 FIGURE:3. This structure not only solves the difficult problem of processing bias circuits but also efficiently realizes odd-order frequency multiplication. After machining and electrical installation, the highest measured output power is 3.1 mW at 221 GHz, and the output power exceeds 2 mW across frequencies ranging from 219 to 227 GHz.

Following the tripler is a 440 GHz sub-harmonic mixer [18], shown in Figure 3(b). An anti-parallel pair of Schottky diodes serves as the key component in the mixer. The diode length is 74 μm, and the cutoff frequency exceeds 8000 GHz. The suspended microstrip matching circuit is built on quartz, and the metal block is cut into two halves. The diode package and matching circuit are integrated in the mixer model. Measured results indicate that the loss is below 17.0 dB in the band ranging from 433 to 451 GHz, with a 3 dB bandwidth of 18 GHz.

The digital subsystem is a high-speed digital correlator. This correlator solves the phase synchronization problem using a cross-synchronization scheme based on a low-cost FPGA controller. After digital quantization, quadrature digital down-conversion is employed to eliminate quadrature error. In this correlator, the sampling rate can reach as high as 5 GHz, the effective number of ADC bits is greater than or equal to 6 [23], and the integration time is adjustable.

### B. Point-source Target Calibration

This SMMW interferometric radiometer has only one elementary interferometer. Therefore, errors originating in the receivers can be regarded as a simple modulation of the source image, as long as the errors remain steady during one imaging period—easily guaranteed by this system. The most crucial error source comes from the flexible waveguide connections employed to complete spatial frequency domain scanning. To address this problem, a point-source target calibration method is presented.

During each imaging period, the system follows the same moving trace. The error from the flexible waveguides can be described as a function of coordinates in the spatial frequency domain. Let *A(u,v)* and  *(u,v)* denote the magnitude and phase errors, respectively. Then Eq. (2) becomes:

$$V(u,v) = \iint_{\xi^2+\eta^2\leq 1} T(\xi,\eta)\cdot F^*_{1,2}(\xi,\eta)\cdot r_{1,2}(\xi,\eta)\cdot \tilde{r}(u,v)\cdot A(u,v)\cdot e^{-j[2\pi(u\xi+v\eta)+\varphi(u,v)]}\, d\xi\, d\eta$$

When considering a point-source target located at *( , )*, we have:

$$V_{ps}(u,v;\xi_0,\eta_0) = \iint_{\xi^2+\eta^2\leq 1} T_p(\xi,\eta)\cdot\delta(\xi-\xi_0,\eta-\eta_0)\cdot F^*_{1,2}(\xi,\eta)\cdot r_{1,2}(\xi,\eta)\cdot \tilde{r}(u,v)\cdot A(u,v)\cdot e^{-j[2\pi(u\xi+v\eta)+\varphi(u,v)]}\, d\xi\, d\eta$$

where *T_p* is the background brightness of the point source. A flat target response can be obtained by turning off the point source:

$$V_{ft}(u,v) = \iint_{\xi^2+\eta^2\leq 1} T_r'(\xi,\eta)\cdot F_{1,2}^*(\xi,\eta)\cdot r_{1,2}(\xi,\eta)\cdot \tilde{r}(u,v)\cdot A(u,v)\cdot e^{-j[2\pi(u\xi+v\eta)+\varphi(u,v)]}\, d\xi\, d\eta$$

where $T\_r$' is the instrument temperature during flat target imaging [24], which may differ from other imaging scenarios. The flat target response serves as flat target calibration for Eq. (4):

$$V_{ps}'(u,v;\xi_0,\eta_0) = V_{ps}(u,v;\xi_0,\eta_0) - V_{ft}(u,v)$$

The influence of the fringe washing function can be neglected. The weighting effect of the antenna pattern becomes approximately constant and close to 1, which can also be ignored. Then Eq. (6) can be used as point-source target calibration for common measurements as described in Eq. (3):

$$V_{ps}''(u,v;\xi_0,\eta_0) = \frac{V_{ps}'(u,v;\xi_0,\eta_0)}{V_{ft}'(u,v)} \approx e^{-j2\pi(u\xi_0+v\eta_0)}$$

where the calibrated result can be regarded as a space shift of the raw visibility function. Furthermore, the relationship between flat target transformation and point-source target transformation is delicate. In theory, the Dirac delta function and constant function are a Fourier transform pair. Thus, the visibility function of a flat target approximates a delta function, while the visibility function of a point-source target resembles a constant function.

In practical application, flat target calibration is an additive operation aimed at minimizing the impact of antenna errors by minimizing $T\_r$ described in Eq. (2). Point-source target calibration is a multiplicative operation used to eliminate multiplicative error. These two calibrations do not interfere with each other. Indeed, flat target calibration assists point-source target calibration in eliminating the influence of instrument temperature, as shown in Eq. (6).

Generally, flat target calibration can work for all synthetic aperture interferometric radiometers, while point-source target calibration is effective for time-sharing systems with a scanning period. However, when introduced to complex systems with more than one elementary interferometer, the inconsistency between receivers should be considered in Eq. (6) and Eq. (7).

---

## 3 Experiment

### A. Interferometric Fringes Experiment

With the interferometer baseline fixed and the point source moving in the horizontal direction of the baseline, interferometric fringes can be obtained as shown in Figure 4 FIGURE:4. The phase of the interferometric fringes is shown in Figure 4(b). During the experiment, the SMMW interferometer operates at 440 GHz, the baseline length is 59.52 mm, and the vertical distance between the interferometer and point source is 1100 mm. From Eq. (1), the displacement corresponding to one interferometric fringe period is 12.6 mm, while the measured value is 12.4 mm. The linear correlation coefficient of the interferometric fringes exceeds 0.999, and the corresponding linear phase error is better than 2°.

### B. Point Source Imaging

Fixing the location of the point source and scanning the spatial frequency domain can be completed by moving the arms of the two-dimensional platform. The SMMW interferometric radiometer operates at 440 GHz, with the longest baseline at 70  in both $u$ and $v$ directions. The primary retrieved image is shown in Figure 5 FIGURE:5, and the point-source target calibrated image using Eq. (7) is shown in Figure 5(c-d).

For theoretical analysis, the normalized synthetic aperture array factor function for an even sampling grid in the spatial frequency domain can be described as:

$$D(\xi, \eta) = \frac{\sin[(2N-1)\pi\xi\Delta u]}{\sin(\pi\xi\Delta u)} \cdot \frac{\sin[(2M-1)\pi\eta\Delta v]}{\sin(\pi\eta\Delta v)}$$

where $\Delta u$ and $\Delta v$ are the minimum antenna spacing normalized to the wavelength in the  and  directions, respectively. $N$ and $M$ are the numbers of antennas in the  and  directions for a non-sparse array. Angular resolution can be defined as the 3 dB beamwidth of the synthetic aperture antenna pattern, with reference to the real aperture system, which is derived from Eq. (8):

$$\theta_{HP} \approx \frac{1.207}{(2N-1)\Delta u}$$

A similar result can be obtained in the  direction.

In this SMMW interferometric radiometer, which comprises a sparse mobile array, the equivalent antenna array corresponds to $N = M = 13$. Introducing these parameters into Eq. (8), the theoretical angular resolution is 0.55°, and the ideal first sidelobe level approaches -6.5 dB. The practical angular resolution is 0.57° as shown in Figure 5(c), which agrees well with theoretical results. In the raw retrieved image, the first sidelobe level is -2.8 dB as shown in Figure 5(a). After point-source target calibration, it decreases to -5.3 dB.

Experimental results demonstrate that point-source target calibration plays a key role in reducing the first sidelobe, which reflects the system errors of the synthetic aperture interferometric radiometer. Unfortunately, there remains an obvious gap between the calibrated image and theoretical image, suggesting that some considerable errors are still hidden in the point-source target calibrated results, which must be addressed in future work.

---

## 4 Conclusion

In this paper, a SMMW interferometric radiometer has been established using a two-element interferometer, and point-source target calibration has been applied to improve radiometer performance. Interferometric fringes and point source images have been presented, with the linear phase error of interference fringes better than 2°. The angular resolution of imaging is 0.57°. System performance shows good agreement with theoretical results.

This interferometer demonstrates the technical feasibility of synthetic aperture imaging in the SMMW spectral region. The results provide an important reference for the next stage of the GIMS project.

For future work, the calibration method should be improved to further reduce system errors. Additionally, a modified SMMW interferometric radiometer is currently under development, and area target imaging is expected.

---

## References

[1] A. Maestrini, J. S. Ward, J. J. Gill, H. S. Javadi, E. Schlecht, C. T. Canseliet, "A 540–640-GHz High-Efficiency Four-Anode Frequency Tripler," *IEEE Transactions on Microwave Theory and Techniques*, vol. 53, no. 9, pp. 2835-2843, Sep. 2005.

[2] K. Leong, X. B. Mei, W. Yoshida, M. Lange, A. Zamora, B. Gorospe, "Progress in InP HEMT Submillimeter Wave Circuits and Packaging," in *IEEE Compound Semiconductor Integrated Circuit Symposium*, New Orleans, LA, 2015, pp. 1-4.

[3] Y. D. Zhang, Y. S. Jiang, Y. T. He, H. Y. Wang, "Passive millimeter-wave imaging using photonic processing technology," *J. Infrared Millim. Waves*, vol. 30, no. 6, Dec. 2011.

[4] A. Luukanen, T. Kiuru, M. M. Leivo, A. Rautiainen, J. Varis, "Passive three-colour submillimetre-wave video camera," *Proc. of SPIE*, vol. 8715, 2015.

[5] Y. Irimajiri, T. Manabe, S. Ochiai, H. Masuko, T. Yamagami, Y. Saito, N. Izutsu, T. Kawasaki, M. Namiki, "BSMILES—A Balloon-Borne Superconducting Submillimeter-Wave Limb-Emission Sounder for Stratospheric Measurements," *IEEE Geoscience and Remote Sensing Letters*, vol. 3, no. 1, Jan. 2006.

[6] H. M. Pickett, R. L. Poynter, E. A. Cohen, "Submillimeter, millimeter, and microwave spectral line catalog," *J. Quant. Spectrosc. Radiat. Transf.*, vol. 60,

no. 5, pp. 883–890, 1998.

[7] J. W. Waters, L. Froidevaux, R. S. Harwood, "The Earth Observing System Microwave Limb Sounder (EOS MLS) on the Aura satellite," *IEEE Trans. Geosci. Remote Sens.*, vol. 44, no. 5, pp. 1075–1092, May 2006.

[8] K. Kikuchi, T. Nishibori, S. Ochiai, "Overview and early results of the Superconducting Submillimeter-Wave Limb-Emission Sounder (SMILES)," *J. Geophys. Res.*, vol. 115, no. D23, pp. D23306-1–D23306-12, Dec. 2010.

[9] H. Liu, J. Wu, S. W. Zhang, "Conceptual design and breadboarding activities of geostationary interferometric microwave sounder (GIMS)," in *Proc. IGARSS*, Cape Town, South Africa, 2009, pp. 1039–1042.

[10] C. Zhang, H. Liu, J. Wu, S. W. Zhang, J. Y. Yan, "Imaging Analysis and First Results of the Geostationary Interferometric Microwave Sounder Demonstrator," *IEEE Trans. Geosci. Remote Sens.*, vol. 53, no. 1, pp. 207–218, Jan. 2015.

[11] W. G. Read, Z. Shippony, M. J. Schwartz, N. J. Livesey, W. V. Snyder, "The Clear-Sky Unpolarized Forward Model for the EOS Aura Microwave Limb Sounder (MLS)," *IEEE Trans. Geosci. Remote Sens.*, vol. 44, no. 5, pp. 1367-1379, May 2006.

[12] F. Rodriguez-Morales, K. S. Yngvesson, E. Gerecht, "A terahertz focal plane array using HEB superconducting mixers and MMIC IF amplifiers," *IEEE Microw. Compon. Lett.*, vol. 15, no. 4, pp. 199–201.

[13] C. S. Ruf, C. T. Swift, A. B. Tanner, and D. M. Le Vine, "Interferometric synthetic aperture microwave radiometry for the remote sensing of the Earth," *IEEE Trans. Geosci. Remote Sens.*, vol. 26, no. 5, pp. 597–611, Sep. 1988.

[14] M. A. Brown, F. Torres, I. Corbella, and A. Colliander, "SMOS Calibration," *IEEE Trans. Geosci. Remote Sens.*, vol. 46, no. 3, pp. 646–658, Mar. 2008.

[15] I. Corbella, F. Torres, A. Camps, A. Colliander, M. M. Neira, S. Ribo, K. Rautiainen, "MIRAS End-to-End Calibration: Application to SMOS L1 Processor," *IEEE Trans. Geosci. Remote Sens.*, vol. 43, no. 5, pp. 1126–1134, May 2005.

[16] A. B. Tanner, W. J. Wilson, B. H. Lambrigsten, "Initial results of the thinned array radiometer (GeoSTAR) demonstrator geostationary synthetic instrument," *IEEE Trans. Geosci. Remote Sens.*, vol. 45, no. 7, pp. 1947–1957, Jul. 2007.

[17] J. Meng, D. H. Zhang, C. H. Jiang, C. F. Yao, "Research on the practical design method of 225 GHz tripler," *J. Infrared Millim. Waves*, Vol. 34, no. 2, pp. 190-195, Apr. 2015.

[18] X. Zhao, C. H. Jiang, D. H. Zhang, C. F. Yao, "Design of the 450 GHz sub-harmonic mixer based on Schottky diode," *J. Infrared Millim. Waves*, Vol. 34, no. 3, pp. 301-306, Jun. 2015.

[19] I. Corbella, N. Duffo, M. Vall-llossera, "The Visibility Function in Interferometric Aperture Synthesis Radiometry," *IEEE Trans. Geosci. Remote Sens.*, vol. 42, no. 8, pp. 1677-1682, Aug. 2004.

[20] R. Butora, M. M. Neira, A. Luis, R. Antich, "Fringe-washing function calibration in aperture synthesis microwave radiometry," *RADIO SCIENCE*, VOL. 38, NO. 2.

[21] A. Camps, J. Bara, I. Corbella, F. Torres, "The Processing of Hexagonally Sampled Signals with Standard Rectangular Techniques: Application to 2-D Large Aperture Synthesis Interferometric Radiometers," *IEEE Trans. Geosci. Remote Sens.*, vol. 35, no. 1, pp. 183-190, Jan. 1997.

[22] C. Zhang, J. Wu, W. Y. Sun, "Applications of Pseudo-polar FFT in Synthetic Aperture Radiometer Imaging," *PIERS Online*, vol. 3, no. 1, 2007.

[23] Q. Z. Wu, C. X. Cai, Y. C. Ding, C. L. Liao, "Design and implementation of 5Gsps high-speed data acquisition system," *Electronic Design Engineering*, vol. 20, no. 1, Jan. 2012.

[24] M. M. Neira, M. Suess, J. Kainulainen, "The Flat Target Transformation," *IEEE Trans. Geosci. Remote Sens.*, vol. 46, no. 3, pp. 613-620, Mar. 2008.

---

**Biography:** Donghao Han (1990-), male, born in Shandong, China, Ph.D. student. Research interests include sub-millimeter wave applications and system design of synthetic aperture radiometers. E-mail: handonghao1124@163.com.

**Foundation Items:** Supported by National 863 Program (2013AA122701) and Scientific Research Fund of Meteorological Public Welfare Profession (GYHY201506023).